Journal of Organometallic Chemistry, 262 (1984) 391–405
Elsevier Sequoia S.A., Lausanne – Printed in The Netherlands

THEORETICAL SEMI-EMPIRICAL STUDY OF CONCERTED OXIDATIVE ADDITIONS TO DINUCLEAR COMPLEXES

A. SEVIN, YU HENGTAI and P. CHAQUIN

Laboratoire de Chimie Organique Theorique. Universite P. et M. Curie, 4 Place Jussieu, 75230 Paris, Cedex 05, Tour 44 (France)

(Received September 15th, 1983)

Summary

A theoretical semi-empirical study of synchronous addition of dihydrogen and acetylene to dimetallic complexes, d^8–d^8 (Rh_2, Ir_2) or d^7–d^7 (Fe_2) is reported. For $(d^8)_2$ complexes, the concerted addition leads to an intermediate diradical which must rearrange before metal–metal bond formation can occur. $(d^7)_2$ complexes react more efficiently; it is shown that cleavage of the initial metal–metal bond may either be concerted with addition in the thermal process or lead to a diradical in the excited state. Thermal and photochemical reactivities are compared in both cases. Competitive addition in the case of $(d^8)_2$ complexes is discussed.

Introduction

Polynuclear complexes of transition metals [1] have recently drawn the attention of both experimental and theoretical chemists [2–12]. Indeed, several cooperating metal centers provide interesting new methods of coordinating and/or activating molecules on the one hand, and on the other hand, the related complexes constitute models for explaining the reactivity observed in homogeneous catalysis and in clusters or on metal surfaces. In this area, the study of concerted additions of small covalent or unsaturated molecules to dinuclear complexes of transition metals (TM2) might be of great help [13–15]. From the vast literature devoted to synthesis, structure and reactivity of TM2 complexes, we have restricted ourselves to a few examples of reactions which might be regarded as oxidative additions. The main experimental trends can be summarized as follows: complexes of $(Rh)_2$ and $(Ir)_2$, $(d^8)_2$ [16–46], or $(Fe)_2$, $(d^7)_2$ [47–62], may yield oxidative addition at two metallic centers, but it is still not clear whether the reaction occurs through a purely concerted pathway or via several steps the first one of which would be oxidative addition to one single metal.

Concerted additions of σ-bonded (like H_2) or π-bonded (like acetylene) molecules to TM2 complexes can be classified according to two types of reactions [63]:

0022-328X/84/$03.00

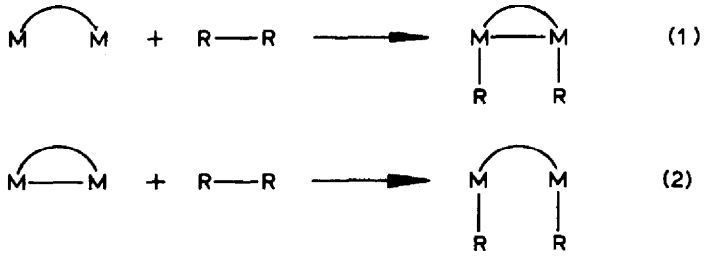

The first one is found with $(d^8)_2$ TM2 complexes such as [Ir(μ-S-t-Bu)(CO)P(OMe_3)$_3$]$_2$ [12,20,25,38,45] and the second one with $(d^7)_2$ complexes like [Fe(μ-SCF_3)$(CO)_3]_2$ [47,57]. Maisonnat and Poilblanc [26] have shown that dihydrogen addition to $(Ir)_2$ complexes is stepwise and primarily occurs at a single center according to the scheme:

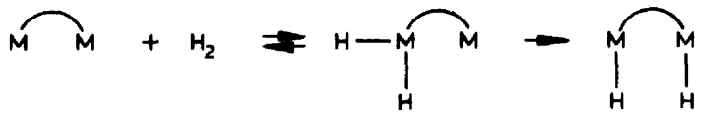

These authors have also shown that bulky ligands can prevent the migration step from occurring, and in that case addition of two dihydrogen molecules, one at each Ir center, is finally observed [62b]. In some cases, addition of acetylenes may require photonic activation [58].

Electronic structures of dinuclear complexes have been studied theoretically by Hoffmann et al. [2–11] and others [50,52,54], but no study of reaction pathways 1 and 2 is available. We propose here an Extended Hückel Theory (EHT) [64] approach to these processes for model $(d^7)_2$ and $(d^8)_2$ compounds. We have chosen H_2 and HCCH as partners in oxidative additions for these molecules are paradigmatic from the dual point of view of energy and spatial MO localization. Indeed this choice brings about arbitrary constraints, but we will see in the following development that it nevertheless allows a general qualitative discussion of the trends encountered in these reactions.

Methods

EHT calculations were performed using an ICON program and the atomic parameters were selected from previous studies [64]. The choice of model structures deserves comment since, for the sake of simplicity, it is convenient to replace the ligands of real complexes by much simpler ones. With this aim, phosphine and carbonyl ligands have been replaced by hydrides, and the S-t-Bu bridging units reduced to SH. Because of these simplifications, an optimization of the geometrical frames would remain meaningless, and in order to emphasize the intrinsic differences between $(Fe)_2$ and $(Ir)_2/(Rh)_2$ complexes, we have adopted for the M_2Z_2 unit a common realistic geometry [65] close to X-ray data [10].

The model reactions are depicted in Fig. 1. In all cases, the C_{2v} point group symmetry is preserved along the reaction pathways, with the given choice of axis. In some cases, variation of the M_2Z_2 ring puckering has been done to test the MO dependence upon M–M distance; this point will be discussed later on.

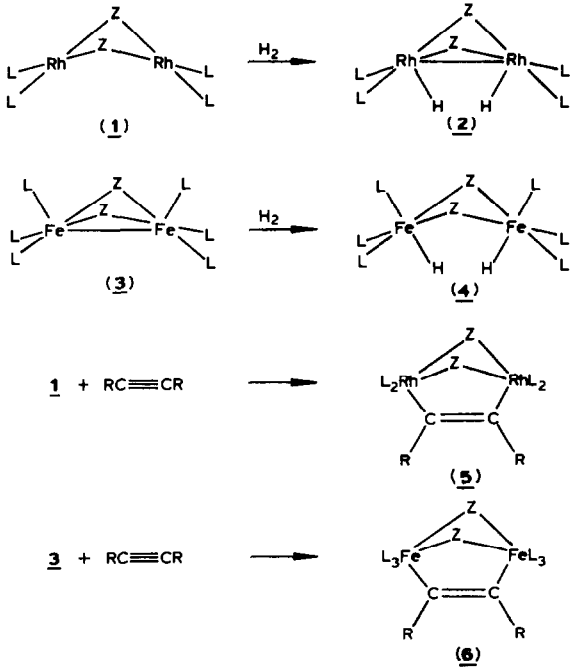

Fig. 1. Model reaction paths. The precise nature of the various L ligands, as well as the bridging species Z, is given in the text. Compounds **1** are related to Rh or Ir as well.

Prior to MO and state analysis of the model reaction paths, let us state some points of general meaning. The reactions presented in Fig. 1 involve several mechanisms: bond making and breaking between metal atoms on the one hand, and between metal and H or C atoms on the other hand. In order to link all these facts, the reasoning used throughout previous discussions of the reactivity of mononuclear TM complexes [66–69] can be transposed with good approximation on the ground of experimental evidence. So, it seems convenient to consider each metal center as potentially oxidizable, leading to MH or MC σ-bonds, where the ligands can be regarded as two-electron ligands (i.e. hydride ions in the case of **2** or **4**, vinyl dianions in **5** or **6**). The last point is easily translated in terms of natural MO correlations [70] and we will now briefly recall the principles that will be used in building the corresponding MO correlation diagrams.

The aforementioned principles rely on three main criteria: (i) preservation of symmetry, (ii) conservation of dominant localization and (iii) conservation of nodal planes. The first pair of criteria is particularly well suited for correlations involving fragments of different electronegativities since the dominant localization is easy to assess, either in the final or the starting system. Once the natural correlations are established, we have to take into account the eventual avoided crossings arising between correlations of the same symmetrey. In a second step, the state-to-state correlation diagram is obtained, taking into account as usual the avoided crossings between states of same symmetry; non monotonic correlations can also result, on a single surface, from avoided crossings found at MO level. To summarize, looking at a given MR bond, we must recall the following simple rule: the corresponding

bonding MO, bearing dominant R character is likely to yield, upon MR stretching, a MO located around R. This point agrees with the chemical picture of oxidative addition where the R ligand is considered as a "two electron ligand" in the final moiety. (It is clear that the reverse process, i.e. breaking of the MR bond follows the same correlation principle.)

MO description of 1 and 3

Before analysing the MO features of reactions 1 and 2, it is necessary briefly to recall the MO description of complexes **1** and **3**, assuming a weak puckering of the M_2Z_2 ring. In other words, this means that the distance between the two metal atoms is large and the overlap of the valence AO's of each metal is very small. Then, in a second step, we will examine the consequences of ring puckering which shortens the MM distance and eventually allows the formation of a MM bond. For the sake of simplicity, we will restrict ourselves to the frontier MO's and consider that all the levels describing the ligands and the metal–ligand bonding or antibonding MO's form two "boxes" of spectator MO's, respectively, occupied or empty, as shown on the left in Fig. 2.

Frontier MO's of complex 1 $(MZL_2)_2$

The frontier set of **1** can be derived from the interaction of the *d*-MO's of two square planar units having local D_{4h} symmetry [10,64,66]. These levels are split as: $e_g(d_{xz}, d_{yz})$, $b_{2g}(d_{xy})$, and, slightly destabilized, $a_{1g}(d_{z^2})$; at higher energy, we find the b_{1g} $(d_{x^2-y^2})$ MO bearing pure antibonding metal-ligand character.

As reported in Fig. 2, we have, in order of increasing energy: (i) a box composed of the set of occupied ligand and metal–ligand bonding MO's, (ii) a set of eight *d*-levels, bearing some minor ligand character and resulting from the duplication of the $e_g + b_{2g} + a_{1g}$ MO's of the square planar units. Under the proper choice of a new axis, and as a result of the weak M–M overlap, we just observe a doubling of the initial levels, resulting in six levels coming from $(e_g + b_{2g})_2$ and two levels coming from $(a_{1g})_2$. Since the *z* axis is common to the mono- and di-nuclear units, we label the latter duo d_{z^2+} and d_{z^2-} to symbolize their in-phase and out-of-phase properties. They are nearly degenerate and, in the case of complex **1**, they are both occupied. At higher energy, we find empty levels, the lowest pair being formed by p_{z+} and p_{z-} in-phase and out-of-phase combinations, respectively, of p_z on each metal (see Fig. 3).

Frontier MO's of complex 3 $(MZL_3)_2$

These MO's are easily derived from the preceding ones by adding two new axial ligands to $(MZL_2)_2$ as depicted in Fig. 3. In the right part of the figure we have two ligand MO's of suitable symmetry, L_{2-}, and in the left part, the MO's of **1** that interact with them the most strongly: $d_{z^2\pm}$ and $p_{z\pm}$. Upon mixing, one gets two σ(ML) bonding MO's (a_1 and b_1 symmetry) having predominantly ligand character. Then we find two $d_{z^2} + p_z$ hybrids pointing out of the ML bonds, and for convenience we still label them $d_{z^2\pm}$. These MO's are quasi-degenerate when the ring puckering is small, but since in the case of **3** they are occupied by only two electrons, it becomes clear that geometrical changes will induce important electronic consequences, as will be seen in the next paragraph.

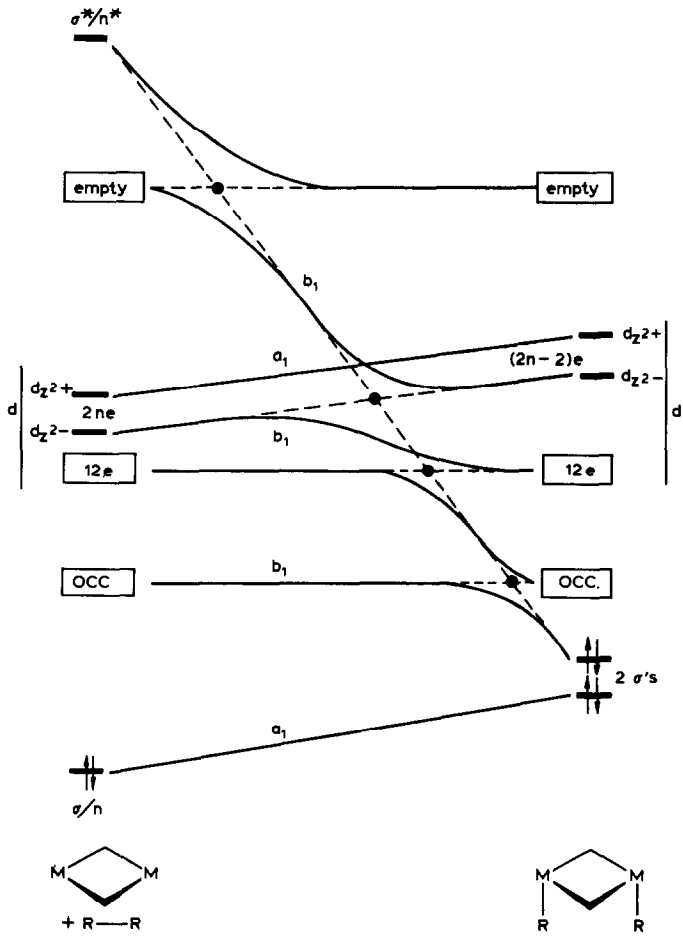

Fig. 2. General MO correlation diagram. The spectator MO's are symbolized by "OCC." and "EMPTY" (see text). n is either 2 for $(Rh)_2$ or $(Ir)_2$ complexes or 1 for $(Fe)_2$. The axes are defined in Fig. 3.

Electronic states of 1 and 3 as a function of ring puckering

Let us examine the relationship existing between the M_2Z_2 ring puckering (or in other words the M–M distance) and the electronic states of these complexes. At a large M–M distance, the $d_{z^2\pm}$ couple is quite degenerate and lies in the same energy range as in the square planar monomer. Upon ring puckering, the M–M distance is shortened and the $\langle d_{z^2}|d_{z^2}\rangle$ overlap increases: d_{z^2+} is stabilized and d_{z^2-} destabilized with respect to the previous situation. This fact, as depicted in Fig. 4, brings about important consequences, and keeping in mind the perturbation theory result stating that upon interaction of two quite degenerate levels, the upper combination (out-of-phase) is more destabilized than the lowest (in phase) is stabilized, we have to consider the total number of electrons in the two $d_{z^2\pm}$ MO's.

(a) When four electrons are present (in complexes like **1**) the system tends to avoid the destabilization of d_{z^2-} and remains nearly planar with a singlet ground state (GS) having the closed shell configuration $^1\{\text{core}(d_{z^2+})^2(d_{z^2-})^2\}$.

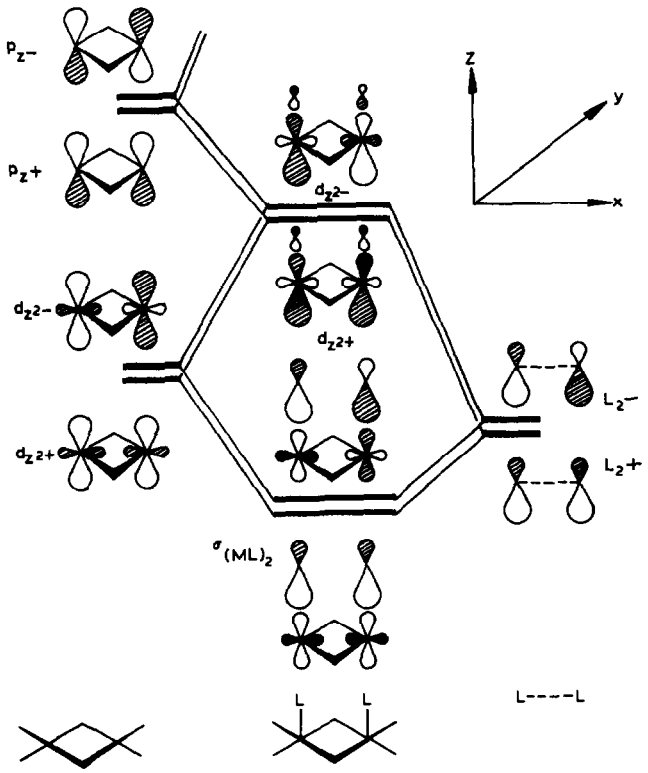

Fig. 3. Perturbation scheme for coupling between two ligands and the set of frontier MO's of adequate symmetry.

(b) When only two electrons are present (in complexes like **3**) the situation is more complex, since we have to accomodate them within two nearly degenerate MO's whose splitting depends on ring puckering.

It is convenient to consider the rest of the electrons of the system as forming a frozen core and to characterize the states of the system according to the electronic configurations of the electrons in $d_{z^2\pm}$. These MO's are of a suitable nature and symmetry to allow the description of an "homosymmetric diradical" according to the terminology of Salem and Rowlands [72]. Of course the following discussion is purely qualitative and relies on analogies with hydrocarbon diradicals and more

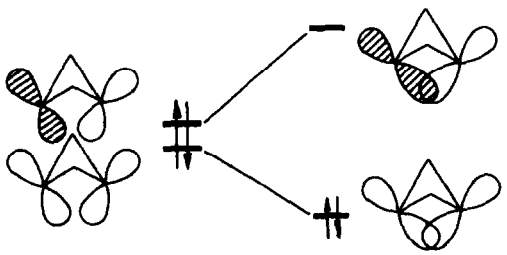

Fig. 4. Variation of the energy of $d_{z^2\pm}$ as a function of ring folding.

particularly on the general fact that in the absence of strongly polar substituents and/or polar solvent, covalent diradicals, i.e. where the two electrons are located on distinct centers, are more stable than ionic (zwitterionic) moieties.

Let us recall briefly the quantum chemical treatment of diradical wavefunctions, applied to the case of $d_{z^2\pm}$. Starting with the situation depicted in the right part of Fig. 4, i.e. when a M–M bond is formed, we can build four electronic configurations: $^1\{\text{core}(d_{z^2+})^2(d_{z^2-})^0\}$ $(^1A_1)$; $^{1,3}\{\text{core}(d_{z^2+})^1(d_{z^2-})^1\}$ $(^{1,3}B_1)$ and $^1\{\text{core}-(d_{z^2+})^0(d_{z^2-})^2\}$, $(^1A_1)$. The first $^1A_1$ state is the closed shell singlet GS of the system and the second $^1A_1$ state is a bi-excited state; if the energy gap separating d_{z^2+} and d_{z^2-} is large enough, these states are also separated by a large energy gap, and even though they have the same symmetry, they do not mix appreciably. The other two states, $^{1,3}B_1$, are mono-excited states, and they do not mix because they have different spin multiplicity, and they do not interfere with the $^1A_1$ states for symmetry reasons $(^1B_1)$ or spin and symmetry reasons $(^3B_1)$; see right side of Fig. 5. The Hartree–Fock energies of these states (assuming M–M bonding) are respectively: E_0 for the GS; $E(^1B_1) - E_o = e_b - e_a - J_{aa} + 2\,K_{ab}$; $E(^3B_1) - E_o = e_b - e_a - J_{ab}$; $E(^1A_1) - E_o = 2(e_b - e_a) - 4\,J_{ab} + 2\,K_{ab} + J_{ab} + J_{bb}$ where a and b stand for d_{z^2+} and d_{z^2-}, respectively, and J and K for the Coulomb and exchange integrals. We see that the relative energies of these states depend (to a first order approximation, i.e. neglecting the J and K terms) on the energies of the $d_{z^2\pm}$ MO's. (In EHT calculations, where J and K are not explicitly calculated, the state energies only depend on e_a and e_b.)

Upon stretching of M–M, the $d_{z^2\pm}$ MO's tend to become quite degenerate, as depicted in the left part of Fig. 4, and the consequences for the preceding states are as follows. (i) The GS of the system is destabilized due to the raising of d_{z^2+}. (ii) The

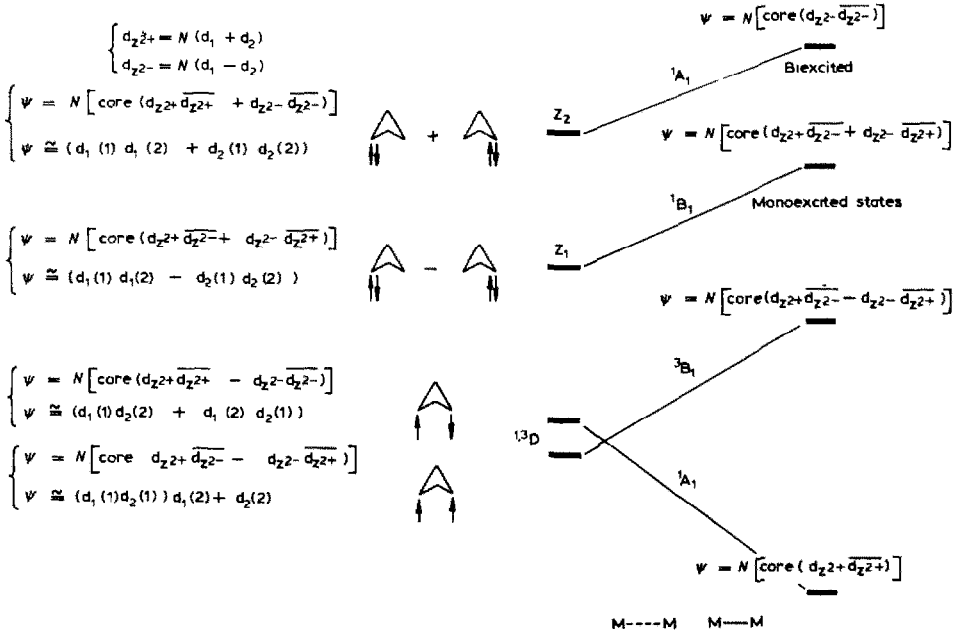

Fig. 5. Qualitative energy variation of the states built on the pair of MO's described in Fig. 4. A more complete description of the corresponding wavefunctions is given in ref. 72.

other three states are stabilized since the $(e_b - e_a)$ term in the energy tends to cancel out. (iii) The energy gap separating the $^1A_1$ states is decreased, and in the final degenerate situation both initial wavefunctions are inadequate to describe the system and we must take their linear combinations, leading to two new $^1A_1$ states:

$$^1\left\{\left(\text{core}(d_{z^2+})^2\right) - \left(\text{core}(d_{z^2-})^2\right)\right\} = {}^1D$$

and

$$^1\left\{\left(\text{core}(d_{z^2+})^2\right) + \left(\text{core}(d_{z^2-})^2\right)\right\} = Z_2$$

It can easily be shown that the first one corresponds to a covalent state [72], where one electron is located on each metal atom, while the second one corresponds to a high energy zwitterion: $\overset{+}{\text{M}}\overset{-}{\text{M}}(+)\overset{-}{\text{M}}\overset{+}{\text{M}}$. (iv) The triplet $^3B_1$ is also covalent and likely to be the GS of the open system; due to the large separation of the metal centers, no important difference can be expected for the singlet and triplet covalent distributions and both states will be found in the same energy range. (v) The singlet $^1B_1$ electronic configuration corresponds to an ionic (zwitterion Z_1): $\overset{+}{\text{M}}\overset{-}{\text{M}}(-)\overset{-}{\text{M}}\overset{+}{\text{M}}$.

The correlations between these states from the initial to the final situation are straightforward as indicated in Fig. 5. Indeed a quantitative calculation of the state energies remains beyond the scope of the study, and we can only predict that, when only two electrons are present in the $d_{z^2\pm}$ pair of MO's, a complexe like **3** can either be regarded as a classical closed shell singlet (at short M–M bond length) or as a diradical (when the M–M distance is large and the overall structure close to a planar geometry).

It is worth noticing that in the case of strongly non-symmetrical complexes of overall structure **3**, the eventual existence of low-lying ionic states can be predicted, as in the case of "sudden polarization" of alkenes [73]; but this is not the place to discuss this point.

MO Correlations and qualitative description of the reactivity

MO Correlations

We have seen that, assuming some labeling simplifications, the MO's of **1** and **3** might be described in an unique fashion. In order to study the oxidative addition process, we have now to deal with the complete starting system which contains, in addition to the aforementioned MO's, those of the R_2 moiety (see Fig. 2). The latter have been reduced for simplicity to $\sigma(R_2)$ and $\sigma^\star(R_2)$ for the model compound H_2; in the case where R_2 = HCCH, these MO's would have to be replaced by the π and $\pi^\star$ pair of a_1 and b_1 symmetry. The final system, apart from the boxes of spectator MO's is composed of: (i) two σ-bonding MO's corresponding to the MR bonds that are formed, (ii) six *d* MO's which are only slightly perturbed during the reaction, and (iii) the $d_{z^2\pm}$ couple which is destabilized by out-of-phase contributions of R_2 during the coupling. The antibonding MO's, counterparts of the bonding ones, have not been drawn since they do not play any role in the forthcoming discussion.

Using the natural orbital correlation principle, the diagram is easily designed. $\sigma(R_2)$ and $\sigma^\star(R_2)$ are correlated with the two bonding MR MO's, as shown by broken lines. The other MO blocks are correlated with the corresponding blocks of the final system [69]; due to symmetry constraints, several avoided crossings occur as

indicated by dots, and, as an end result, we obtain the heavy line correlations. The topology of this diagram is common to all the oxidative processes described in Fig. 1, but the number of electrons that we have to put into the $d_{z^2\pm}$ set depends on the actual metal: 4 for $(Rh)_2$ and $(Ir)_2$ complexes and 2 for the $(Fe)_2$ complexes.

$M_2L_4Z_2$ ($d^8 + d^8$) compounds

The Rh or Ir atoms are d^8 in type **1** complexes. The $d_{z^2\pm}$ pair is filled by four electrons and a metal–metal bond is not likely to exist since the bending, which would bring the metal atoms closer, develops an important destabilization due to the negative overlap in d_{z^2-}. In those complexes, the MM bond is rather long (3.06 for Rh–Rh and 3.21 Å for Ir–Ir) [19,28] and the splitting of the $d_{z^2\pm}$ set is weak. A total of 16*d*-electrons is found in the system. We see that in the final species **2** four electrons are necessary to ensure MR bonding, two of them coming from R_2 and two from the *d* set; we have a $d^7 + d^7$ complex ($Rh^{II} + Rh^{II}$; 7 electrons on each Rh atom) having two electrons in the $d_{z^2\pm}$ couple. We are in the precise case described in Fig. 4 and, in the absence of important geometrical rearrangement, the primary product of the reaction **1** → **2** is more likely to be a diradical **2a** (Fig. 6). Indeed, when the concerted reaction proceeds, the $d_{z^2\pm}$ couple "grows" on the opposite side to the incoming hydrogens, yielding **2a**. (The MO perturbation scheme is the same as previously described in Fig. 3.) To form a M–M bond, the diradical can either invert the MZMZ ring or rearrange its ligands as shown (among other possibilities) in **2b**.

A qualitative evaluation of the various potential energy surfaces (PES's) is depicted in Fig. 7. From the ground state of the starting system, an endothermic reaction involving an activation energy, yields the $^1A_1$ diradical ^1D which may evolve in order to form an M–M bond. A second potential energy barrier is predicted along this portion of the reaction coordinate, for important conformational changes of the ligands are necessary before reaching a geometry favorable to M–M bond formation. In the excited state, $^3B_1$, a triplet surface leads directly to the stable intermediate tripled diradical, which, through inter-system crossing, may yield the final molecule. A non-radiative deactivation channel is found during the addition process, and the competing paths of this state are symbolized by wavy lines. We also see in Fig. 7 that an exothermic reaction may proceed along the mono-excited $^1B_1$ PES, yielding a zwitterionic intermediate possessing a large excess of internal energy with respect to either the initial or the final systems, even though its further evolution is difficult to predict.

It should be clear that, in Fig. 7, we have split the overall reaction into two

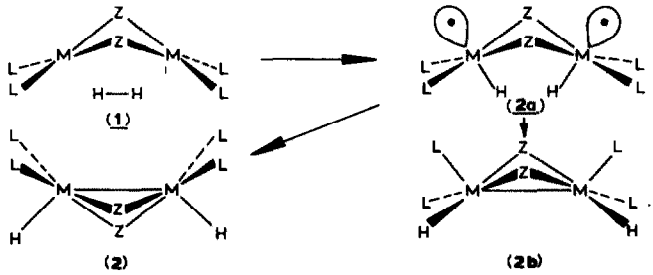

Fig. 6. Geometrical changes imposed by the oxidative addition to complexes of type **1**.

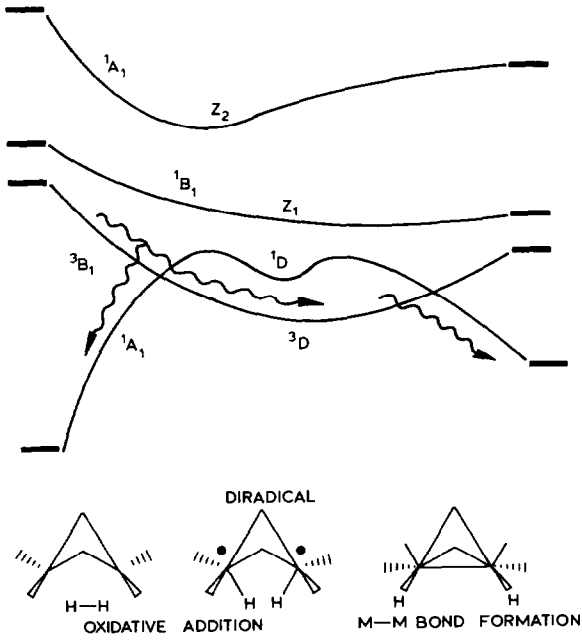

Fig. 7. Qualitative state-correlation diagram corresponding to oxidative addition to compounds **1**. Such a partition of the reaction coordinate is arbitrary and is done in order to emphasize the dominant electronic events occurring along the path. It is clear that in the real process both steps are closely linked.

limiting processes only for the sake of clarity. In reality, both types of motion would be linked, providing a continuous reaction coordinate. Nevertheless, the eventual existence of a stable diradical intermediate on the lowest triplet PES must be emphasized.

$M_2L_6Z_2$ ($d^7 + d^7$) compounds

In complex **3**, where two Fe^I atoms (d^7) are cooperating, two electrons occupy the frontier $d_{z^2\pm}$ pair. For previously invoked reasons, the MZMZ ring is puckered in order to allow the formation of an M–M bond. During the reaction, this bond is broken, and the "open" form is probably involved, at least in the photochemical process. Thus, it is practical to use the state diagram of Fig. 5 to depict this portion of the reaction coordinate, as repeated in the left part of Fig. 8. Starting from the diradical intermediate, the state-to-state correlations are easy to assess, as shown in the right part of the Fig. 8.

GS reactivity. Along the GS PES ($^1A_1$) a weak energy barrier can be predicted during the concerted addition, resulting from the MO avoided crossing previously discussed in Fig. 2, and symbolized in Fig. 8 by a mixing with the upper bi-excited configuration Z_2 of the same symmetry. The ^1D diradical may now capture dihydrogen to yield the final product. Obviously this partition of the reaction coordinate is somewhat arbitrary, since both M–M bond rupture and M–H bond formation may be synchronous, but it has the merit of showing that a stable intermediate may be formed, more especially in the excited state, prior to dihydrogen addition. We have

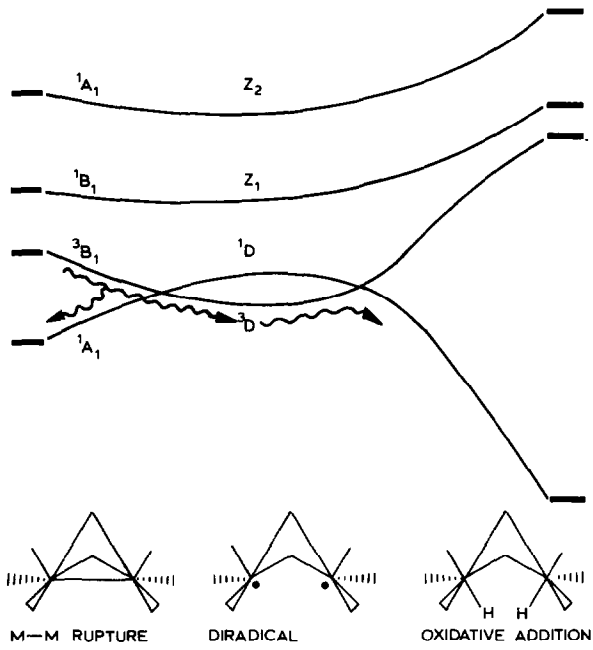

Fig. 8. Qualitative state correlation diagram for oxidative addition to **3**. (The same remark applies as for Fig. 7).

carried out calculations for this model reaction path and the results are shown in Fig. 9.

The potential energy is drawn as a function of the H–H distance (horizontal axis) and of the distance between the middles of the H–H and Fe–Fe segments (C_{2v} point group). A realistic reaction path is depicted by the arrows; two facts emerge. (i) During the major part of the reaction coordinate the H–H distance remains almost constant, at its equilibrium value. Then a very fast stretching appears "catastrophically" near to the saddle point. A similar result has already been found and discussed for oxidative addition to a mononuclear complex [68]. (ii) The activation energy, at EHT level, is very weak (0.2 eV), clearly showing that once the H_2 molecule is close to the di-metal system, cleavage of the metallic bond and of H_2 is neatly balanced by the formation of two Fe–H bonds. Contrary to the case of $M_2L_4Z_2$ complexes, the reaction does not require important geometrical changes and corresponds roughly to a least-motion process.

Lowest triplet state reactivity. As shown in Fig. 8, the lowest triplet state of **3** exothermally yields the triplet diradical through breaking of the Fe–Fe bond. Once formed, this diradical is not directly reactive and reclosure of the system will compete with inter-system crossing leading to the final molecule (wavy lines), with a large excess of internal energy. As we have already noted it is difficult to predict the reactivity of the highest excited states, except the fact that the Z_1 species cannot directly yield the final system, but requires an internal conversion $^1B_1 \rightarrow {}^1A_1$ competing with deactivation leading to a "hot" system.

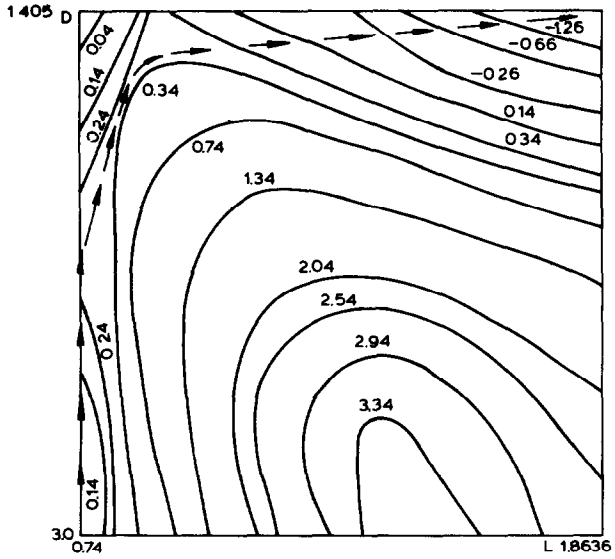

Fig. 9. EHT calculated potential energy surfaces for addition of H_2 to the model compound $(Fe(H)_3SH)_2^{6-}$. A realistic pathway is outlined by arrows. The horizontal axis refers to H–H stretching (L) and the vertical one to the distance (D) between the middles of M–M and H–H.

Acetylene vs. hydrogen addition

There is no qualitative difference between the correlation diagrams drawn for H_2 or HCCH addition. Nevertheless, several remarks can be made.

(i) From a thermodynamical point of view, the energy of the π-bond to be broken is lower than the H_2 one. In MO terms, this means that, in Fig. 2, the destabilization of the lowest σ/π MO will be less for acetylene than for hydrogen addition.

(ii) The CC bond length of acetylene and the spatial extention of the π and $\pi^\star$ MO's allow a good overlap at the beginning of the reaction coordinate. From this point of view, a better reactivity can be expected for acetylene.

(iii) On the other hand, the inversion of the MZMZ ring **2a** → **2** (Fig. 6) is impossible for the acetylene adduct. Formation of the M–M bond thus requires a rearrangement of the ligands according to the **2a** → **2b** reaction path.

(iv) Moreover, the presence of another empty $\pi^\star$ MO (a_2 symmetry) acts as a supplementary stabilization factor. This is confirmed by model calculations, since the **3** $(d^7)_2$ + HCCH → **6** reaction appears almost spontaneous at EHT level.

Competition between one center and two center oxidative addition to $(d^8)_2$ complexes

In the preceding paragraph we have pointed out that synchronous additions of H_2 or RCCR′ (to $(d^8)_2$ complexes of Rh or Ir lead to $(d^7)_2$ open-shell diradicals and require important ligand rearrangements before M–M bond formation can occur. It is therefore clear that these processes are in competition with oxidative additions at one single center leading to a $(d^6 + d^8)$ system. A series of arguments can be invoked in favor of this mechanism.

(i) If the initial structure of the complex is nearly planar, one can consider to a first approximation that the metal centers are independent and that the reaction may

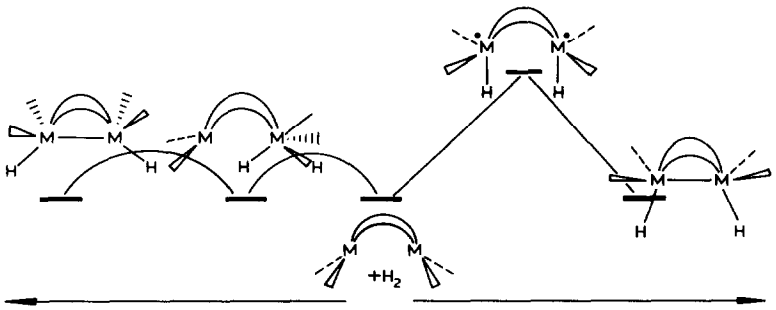

Fig. 10. Qualitative scheme describing the various energy changes along the concerted addition (right) and two step addition (left).

proceed as in the usual case of oxidative addition to a d^8 metal. This reaction which involves a low activation energy, from 10 to 20 kcal/mol [74] leads to a d^6 stable closed-shell octahedral complex. In the case of $(TM)_2$ complexes, we might consider that the same range of activation energy will be found, considering that the "spectator" metal is not significantly involved in the overall process.

(ii) For monometallic catalysts, oxidative dihydrogen addition is slightly exothermic [75]. If we transfer this argument to the case of $(TM)_2$ complexes, we can conceive that addition to a single center is thermodynamically favored since we get finally a small energy gain at one center and no change at the other, while in the case of concerted addition at two centers we have an overall endothermic process leading primarily to a diradical intermediate.

(iii) The primary product resulting from oxidative addition at a single center might transfer one hydrogen atom from one metal to the other in a second step. This reaction requires ligand rearrangement and it is conceivable that steric effects might play an important role, as observed experimentally [26].

The qualitative scheme of Fig. 10 resumes the discussion.

Conclusion

The thermal concerted addition appears to be much easier for d^7–d^7 $(Fe)_2$ than for d^8–d^8 $(Rh/Ir)_2$ complexes. Indeed, in the latter case, an energy barrier results from an allowed HOMO/LUMO crossing (Fig. 2). We can see in Fig. 2 that this reaction requires the initial destabilization of two filled MO's (d_{z^2+} and d_{z^2-}). Moreover, once the diradical **2a** is formed, a rearrangement of the ligands or a ring inversion is necessary to reach the final M–M bonded structure. So, a two-step mechanism, with preliminary oxidative addition at a single metal atom, appears more realistic, in agreement with experimental results. These difficulties are not encountered in the thermal concerted additions to d_7–d_7 $(Fe)_2$ systems, and we believe that this possibility must not be a priori ruled out, especially in acetylene addition.

Regarding photochemical reactivity, a triplet diradical is likely to be an intermediate during the addition to $(d^7)_2$ complexes and after addition to $(d^8)_2$ complexes. The proximity to this species of the singlet diradical surface, correlated to the GS of both initial and final products, presumably allows an efficient

inter-system crossing: there are two competing reactive and non-reactive channels, and it is difficult, in this semi-empirical study, to evaluate their respective quantum yields; but we want to point out that photochemical activation might lead quite efficiently to reaction.

Acknowledgment

The authors are greatly indebted to Prof. R. Poilblanc for stimulating discussions.

References and notes

1 See, for example, F.A. Cotton and R.A. Walton, Multiple Bonds Between Metal Atoms, Wiley, New York, 1982.
2 P.J. Hay, J.C. Thibeault and R. Hoffmann, J. Am. Chem. Soc., 97 (1975) 4884.
3 R.H. Summerville and R. Hoffmann, J. Am. Chem. Soc., 98 (1976) 7240.
4 D.L. Thorn and R. Hoffmann, Inorg. Chem., 17 (1978) 126.
5 A. Dedieu and R. Hoffmann, J. Am. Chem. Soc., 100 (1978) 2074.
6 P.L. Mehrotra and R. Hoffmann, Inorg. Chem., 1978, 17, 2187.
7 T.A. Albright and R. Hoffmann, J. Am. Chem. Soc., 100 (1978) 7736.
8 A.R. Pinhas and R. Hoffmann, Inorg. Chem., 18 (1979) 654.
9 R.H. Summerville and R. Hoffmann, J. Am. Chem. Soc., 101 (1979) 3821.
10 D.M. Hoffman, R. Hoffmann and C.R. Fisel, J. Am. Chem. Soc., 104 (1982) 3858.
11 D.M. Hoffman and R. Hoffmann, Organometallics, 1 (1982) 1299.
12 A. Serafini, R. Poilblanc and J.F. Labarre, Theor. Chim. Acta, 50 (1978) 159.
13 R. Poilblanc, Nouveau J. Chim., 2 (1982) 145.
14 R. Poilblanc, J. Organomet. Chem., 94 (1975) 241.
15 E.L. Muetterties, W.R. Pretzer, M.G. Thomas, B.F. Beier, D.L. Thorn, W.W. Day and A.B. Anderson, J. Am. Chem. Soc., 100 (1978) 2090.
16 L.F. Dahl, C. Martell and D.L. Wampler, J. Am. Chem. Soc., 83 (1961) 1761.
17 J.A. Ibers and R.G. Snyder, Acta Crystallogr., 15 (1962) 923.
18 A. Maisonnat, P. Kalck and R. Poilblanc, Inorg. Chem., 13 (1974) 661.
19 P. Kalck and R. Poilblanc, Inorg. Chem. 14 (1975) 2779.
20 J.J. Bonnet, P. Kalck and R. Poilblanc, Inorg. Chem., 16 (1977) 1514.
21 A. Thorez, A. Maisonnat and R. Poilblanc, J. Chem. Soc., Chem. Commun., (1977) 518.
22 J.J. Bonnet, J. Galy, D. de Montauzon and R. Poilblanc, J. Chem. Soc., Chem. Commun. (1977) 47.
23 C.P. Kubiak and R. Eisenberg, J. Am. Chem. Soc., 99 (1977) 6129.
24 W.A. Herrmann, C. Krüger, R. Goddard and I. Bernal, Angew. Chem. Int. Ed. Engl., 16 (1977) 334.
25 P. Hofmann, Angew. Chem. Int. Ed. Engl., 16 (1979) 554.
26 A. Maisonnat and R. Poilblanc, J. Organomet. Chem., 160 (1978) 307.
27 M.D. Curtis, W.M. Butler and J. Greene, Inorg. Chem., 17 (1978) 2928.
28 A.J. Sivak and E.L. Muetterties, J. Am. Chem. Soc., 101 (1979) 4878.
29 J.J. Bonnet, A. Thorez, A. Maisonnat, J. Galy and R. Poilblanc, J. Am. Chem. Soc., 101 (1979) 5940.
30 M. Cowie and S.K. Dwight, Inorg. Chem., 18 (1979) 2700.
31 M. Cowie and T.G. Southern, J. Organomet. Chem., 193 (1980) C46.
32 C.P. Kubiak and R. Eisenberg, Inorg. Chem., 19 (1980) 2726.
33 C.P. Kubiak and Eisenberg, J. Am. Chem. Soc., 102 (1980) 3637.
34 W.A. Herrmann, J. Plank, M.L. Ziegler and B. Balbach, J. Am. Chem. Soc., 102 (1980) 5908.
35 J. Devillers, J.J. Bonnet, D. de Montauzon, J. Galy and R. Poilblanc, Inorg. Chem., 19 (1980) 154.
36 C.P. Kubiak C. Woodcock and R. Eisenberg, Inorg. Chem., 19 (1980) 2733.
37 W.A. Herrmann, C. Bauer, J. Plank, W. Kalcher, D. Speth and M.L. Ziegler, Angew. Chem. Int. Ed. Engl., 20 (1981) 193.
38 K.H. Theopold and R.G. Bergman, J. Am. Chem. Soc., 103 (1981) 2489.
39 M. Cowie and R.S. Dirkson. Inorg. Chem., 20 (1981) 2682.
40 W.A. Herrmann, J. Plank, D. Riedel, M.L. Ziegler, K. Weidenhammer, E. Guggolz and B. Balbach, J. Am. Chem. Soc., 103 (1981) 63.

41 R.R. Burch, E.L. Muetterties, R.G. Teller and J.M. Williams, J. Am. Chem. Soc., 104 (1982) 4257.
42 E.B. Meier, R.R. Burch, E.L. Muetterties and V.W. Day, J. Am. Chem. Soc., 104 (1982) 2661.
43 H. Werner and J. Wolf, Angew. Chem. Int. Ed. Engl., 21 (1982) 296.
44 W.A. Herrmann, Pure Appl. Chem. 54 (1982) 65.
45 P. Kalck, J.J. Bonnet and R. Poilblanc, J. Am. Chem. Soc., 104 (1982) 3069.
46 M. El Amane, R. Mathieu and R. Poilblanc, Nouveau J. Chim., 6 (1982) 191.
47 R.F. Bryan, P.R. Greene, M.J. Newlands and D.S. Field, J. Chem. Soc. A, (1970) 3068.
48 J.L. Davidson, W. Harrison, D.W.A. Sharp and G.A. Sim, J. Organomet. Chem., 46 (1972) C47.
49 M.J. Bennett, W.A.G. Graham, R.P. Stewart, Jr. and R.M. Tuggle, Inorg. Chem., 12 (1973) 2944.
50 B.K. Teo, M.B. Hall, R.F. Fenske and L.F. Dahl, Inorg. Chem., 14 (1975) 3103.
51 D.C. Harris and H.B. Gray, Inorg. Chem., 14 (1975) 1215.
52 A.B. Anderson, Inorg. Chem., 15 (1976) 2598.
53 K. Fauvel, R. Mathieu and R. Poilblanc, Inorg. Chem., 15 (1976) 976.
54 J.K. Burdett, J. Chem. Soc., Dalton Trans., 1977, 423.
55 J.P. Collman, R.K. Rothrock, R.G. Finke and F.R. Munch, J. Am. Chem. Soc., 99 (1977) 7381.
56 P.A. Wegner, V.A. Uski, R.P. Kiester, S. Dabestani and V.W. Day, Inorg. Chem., 99 (1977) 4846.
57 G. Le Borgne, D. Grandjean, R. Mathieu and R. Poilblanc, J. Organomet. Chem., 131 (1977) 429.
58 R. Mathieu and R. Poilblanc, J. Organomet. Chem., 142 (1977) 351.
59 C.E. Summer, Jr., P.E. Riley, R.E. Davis and R. Pettit, J. Am. Chem. Soc., 102 (1980) 1752.
60 C.P. Casey, P.J. Fagan and W.H. Miles, J. Am. Chem. Soc., 104 (1982) 1134.
61 V.W. Day, D.A. Lesch and T.B. Rauchfuss, J. Am. Chem. Soc., 104 (1982) 1290.
62 (a) K.M. Motyl, J.R. Morton, C.K. Schaver and O.P. Anderson, J. Am. Chem. Soc., 104 (1982) 7325; (b) E. Guilmet, A. Maisonnat ane R. Poilblanc, submitted for publication.
63 R. Poilblanc, Inorg. Chim. Acta, 62 (1982) 75.
64 (a) R. Hoffmann, J. Chem. Phys., 39 (1963) 1397; (b) R. Hoffmann and W.N. Lipscomb, ibid., 36 (1962) 2179; (c) idem ibid., 37 (1962) 2872.
65 The atomic parameters were taken from previous EHT calculations, especially those in ref. 3. This geometry has the following parameters: M–H 1.6, M–S 2.356, S–H 1.34 Å; SMS 82.31°; four-membered ring puckering 130°, M–M 3.216 Å.
66 R. Hoffmann, M.M.L. Chen and D.L. Thorn, Inorg. Chem., 16 (1977) 503.
67 A. Dedieu and A. Strich, Inorg. Chem., 18 (1979) 2940.
68 A. Sevin, Nouveau, J. Chim., 5 (1981) 233.
69 A. Veillard, Nouveau J. Chim., 5 (1981) 599.
70 A. Devaquet, A. Sevin and B. Bigot, J. Am. Chem. Soc., 100 (1978) 2009.
71 In the case of oxidative addition to **3**, the final MO's corresponding to $d_{z^2\pm}$ belong to a set of antibonding levels.
72 L. Salem and C. Rolands, Angew. Chem. Int. Ed. Engl., 11 (1972) 92.
73 L. Salem, Acc. Chem. Res., 12 (1979) 87.
74 See a review of this problem, in B.R. James, Homogeneous Hydrogenation, Wiley, 1973.
75 (a) J.O. Noell and P.J. Hay, J. Am; Chem. Soc., 104 (1982) 4578; (b) K.K. Taura, S. Dbara and K. Morokuma, ibid., 103 (1981) 2891, and references therein.